EARTHQUAKE GROUND MOTION NEAR THE SOURCE

by

A. K. Mal[I] and A. R. Carriveau[II]

SYNOPSIS

Using a simple two dimensional model of the San Fernando earthquake, the SH component of the ground motion produced in the epicentral region is calculated. A kinematic model of the rupture which is consistent with the mode III deformation of fracture mechanics is used as a model of the propagating fault. The calculated displacement spectrum agrees well with that of the recorded motion at Pacoima Dam.

INTRODUCTION

Most shallow earthquakes occur by a sudden shear failure of the earth material. The failure usually begins at a point on a preexisting fault surface and spreads across with speeds of the order of a few kilometers per second. The ground motion in an earthquake is caused by the elastic waves which are created by the suddenly appearing discontinuity along the fault.

Suitable mathematical models of the source and the ground subsurface must be used in the analysis of the earthquake records. Most of the models which exist in the literature to date have been proposed in connection with seismological studies. The seismological model of an earthquake usually consists of a point source of dislocation embedded in a layered earth, which may be either flat or spherical. Since the major objective of the seismologists is the determination of the earth's internal structure from the analysis of the far-field data, the point source model of the source is adequate for their purpose. The recording and analysis of strong ground motion is one of the major objectives in earthquake engineering. The ground motion is usually the strongest in the vicinity of the source. The nature of this motion is, in general, dependent upon the properties of the source as well as those of the soil between the source and the site. It is, however, reasonable to expect that the source will have a predominant effect on the near field motion. Thus a detailed knowledge of the source mechanism is an essential ingredient in the analysis

I Associate Professor, School of Engineering and Applied Science, University of Calif., Los Angeles, Calif. 90024

II Graduate Student, University of California

of strong motion data. Consequently, the seismologist's model of the earthquake source is inadequate for this purpose.

The literature on the calculation of strong ground motion produced by realistic fault models is rather sparse. Haskell (1969) and Haskell and Thomson (1972) calculated the near field motion due to finite propagating faults in an infinite medium. Mal (1972)* calculated the Rayleigh waves generated on the surface of a half-space in a simple two dimensional model of the 1971 San Fernando earthquake. All of these authors used kinematic models of faulting which are inconsistent with the theories of fracture. Although the precise mechanism of earthquake fault rupture is not known, the mechanics of the fracture of brittle elastic materials have been studied in detail by researchers in fracture mechanics (see, e.g., Eshelby, 1971). In this paper we consider the two dimensional model of I and calculate the ground motion produced by the anti-plane shear component of the propagating fault. By using a kinematic model of faulting consistent with the mode III deformation of fracture mechanics, we show that the simple model of I is adequate for the calculation of strong ground motion in the epicental region.

THEORY

The two dimensional model of the half space together with the coordinate axes (x_1, x_2, x_3) and (ξ_1, ξ_2, ξ_3) are shown in figure (1a). $x_2=0$, $-\infty < x_1, x_3 < \infty$, is the free surface of the half space, and $\xi_2 = 0$, $0 < \xi_1 < \ell$, $-\infty < \xi_3 < \infty$ is the fault surface. The rupture is assumed to begin at the focus S and to propagate with speed c along SA until it emerges at the free surface at A. In the mode III deformation considered here, there is only one nonzero component of the displacement vector which is denoted by $u(\underline{x},t)$, where $\underline{x}=(x_1,x_2)$. We denote by $f(\xi_1,t)=[\overline{u}(\xi_1,t)]$ the jump in the displacement across the fault SA. Let $U(\underline{x},w)$ and $F(\xi_1,\omega)$ be the Fourier time transforms of $u(\underline{x},t)$ and $f(\xi_1,t)$, defined by the formula

$$U(\underline{x},\omega) = \int_{-\infty}^{\infty} u(\underline{x},t)\, e^{i\omega t}\, dt .$$

Using the representation theorem given in I and and after some simplification, the transformed displacement on the surface of the half space can be written as,

$$U(\underline{x},\omega) \equiv U(x_1, 0, \omega) = -\, i\frac{\omega}{\beta}(d-x_1)\sin\theta \int_0^{\ell} F(\xi_1,\omega)\, H_1^{(1)}\left(\frac{\omega R}{\beta}\right)/R\, d\xi_1$$

where β is the shear wave velocity of the medium,

*Hereafter referred to as I.

$R^2 = (x_1 - \xi_1 \cos\theta)^2 + (h - \xi_1 \sin\theta)^2$ and $H_1^{(1)}(\ )$ is the Hankel function of the first kind of order 1. d, h and θ are defined in figure (1a). By obvious change of variables the above expression may be written in the form

$$U(x_1, \omega) = -i \frac{\omega d}{\beta} (1-x) \tan\theta \int_0^1 F(\ell\xi, \omega) \frac{H_1^{(1)}\left(\frac{\omega d}{\beta} r\right)}{r} d\xi \qquad (1)$$

where

$$x = x_1/d \qquad (2)$$

and

$$r^2 = (x-\xi)^2 + (1-\xi)^2 \tan^2\theta \qquad (3)$$

In equation (1), $U(x_1, \omega)$ is the unknown surface displacement and $F(\ell\xi, \omega)$ is the jump discontinuity in the displacement across the fault surface SA. The above equation has been obtained under the assumption that the fractured surfaces are traction free. In the rigorous and more realistic formulation of the problem, an integral equation similar to (1) must be obtained by using the proper frictional boundary conditions at the fault surface. The unknown function $F(\xi_1, \omega)$ can then be determined as a solution of the resulting integral equation. This procedure leads to a very complex problem of dynamic fracture theory whose solution is as yet unknown.

For the purpose of the present calculations we shall, as in I, assume the slip function $f(\xi_1, t)$. In I, the discontinuity in the displacement was assumed to be a propagating step of constant speed c, so that the final static displacement along the fault surface was of constant magnitude. Clearly this violates the theory of crack equilibrium in which the shape of the crack must be elliptic near the tip. In the present paper we assume that the shape of the running crack is elliptic (the dashed curves in figure (1b)) and the ultimate displacement is in the form a quadrant (or nearly so) of an ellipse (the solid curve in figure (1b)). If the magnitude of the surface faulting is D, the prescribed jump across SA is given by,

$$\begin{aligned} f(\xi_1, t) &= 0, && t < \xi_1/c \\ &= D\sqrt{\xi_1(ct-\xi_1)}/\ell\sqrt{2n-1}, && \xi_1/c < t < 2n\ell/c \\ &= D\sqrt{\xi_1(2n\ell-\xi_1)}/\ell\sqrt{2n-1}, && t > 2n\ell/c \end{aligned} \qquad (4)$$

where c is the crack speed and $n(> 1/2)$ is an arbitrary number which determines the time of propagation. For $n = 1$, the time of propagation is $2\ell/c$ and the static displacement on the fault surface is given by the quadrant of an ellipse with major axis ℓ and minor axis D. The Fourier transform of the above expression is given by

$$F(\ell\xi,\omega) = \frac{D\ell}{c\sqrt{2n-1}}\sqrt{\xi}\,G(\xi,\Omega) \tag{5}$$

where

$$G(\xi,\Omega) = \frac{i}{2}\frac{\sqrt{2\pi}}{\Omega^{3/2}}e^{i\Omega\xi}\,C(z) + \pi\sqrt{2n-\xi}\,e^{2in\Omega}\,\delta(\Omega) \tag{6}$$

$$\Omega = \omega\ell/c \tag{7}$$

$$z = (2n-\xi)\Omega \tag{8}$$

$\delta(\Omega)$ is the Dirac delta function and $C(z)$ is the Fresnel integral defined by

$$C(z) = \int_0^z \frac{e^{i\lambda}}{\sqrt{2\pi\lambda}}\,d\lambda \tag{9}$$

Then by (1) and (5) the spectral displacement is given in nondimensional form as

$$\bar{U}(x,\Omega) = -\,i\Omega(1-x)\tan\theta\int_0^1 \sqrt{\xi}\,G(\xi,\Omega)\frac{H_1^{(1)}(m\Omega r)}{r}\,d\xi \tag{10}$$

where

$$U(x,\Omega) = Dd\bar{U}(x,\Omega)/\,2\beta\sqrt{2n-1} \tag{11}$$

and

$$m = c\cos\theta/\beta \tag{12}$$

Note that in the above Ω is a dimensionless frequency and m is the horizontal component of the crack speed normalized with respect to the shear wave speed in the medium.

NUMERICAL RESULTS

The spectral displacement in the epicentral region $0 < x < 1$ can be computed from equation (11) if suitable values are assigned to the parameters appearing in the equation. It is, however, desirable that the computed values be compared with the available recorded motion so that the suitability of the assumed simple model in predicting real earthquake motion be examined. Fortunately, the ground acceleration (vertical and horizontal) in the San Fernando earthquake was recorded at Pacoima Dam, which is located approximately at the point P ($x \cong 3/4$) in the assumed model (figure (1a)). The digitized records were obtained from the Caltech Data Processing Center and were Fourier anal-

yzed at UCLA. The horizontal components were rotated to yield the acceleration spectrum in a direction parallel to the fault break, and the spectral displacement was obtained by a division of the acceleration spectra by $-\omega^2$. The real and imaginary parts of the spectral displacement are shown by the dashed curves in figures (2) and (3) respectively. The data are not reliable for $\omega < 0.5$ radians per second, and thus are not plotted in the figures. The solid curves in figures (2) and (3) are the real and imaginary parts of the spectral displacement computed from equation (11) with the following assigned values to the various parameters.

$$x = 0.75$$

$$n = 1$$

$$\theta = 45^{o}$$

$$m = 1/\sqrt{2}$$

$$\frac{Dd}{\beta} = 700 \text{ cm-sec}$$

$$\ell/c = 7 \text{ sec}$$

The numerical computation of the Fresnel integral was performed by using the rational approximation formulas given by Boersma (1960). In spite of the crudeness of the model, and the approximate values of the parameters, the agreement in the general shape and amplitude of computed and the observed spectra is rather remarkable. The disagreement at higher frequencies is probably due to the fact that the soil properties have a stronger influence on the ground motion at these frequencies. The values of the last four parameters give $D \cong 140$ cm. which is in reasonable agreement with the observed permanent horizontal offset in the San Fernando earthquake (c.f. Canitez and Toksöz, 1972).

The agreement can be improved by changing some of the parameters, but this was not done in the present study.

The modulus of the dimensionless displacement $\bar{U}(x, \Omega)$ is plotted against frequency for various locations in the epicentral region in figure (4). The modulus increases and the curves become less jagged as the location of the station moves towards the fault break.

Although equation (9) is valid for points outside the epicentral region, $x < 0$, $x > 1$, computations were not per-

formed for these locations. Calculations were also performed by using two other kinematic models of the source. These were the propagating step (considered in I) and the ramp (considered by Haskell and Thomson). The characteristics of the displacement spectra in these cases were very much different from that of the recorded motion at Pacoima Dam.

ACKNOWLEDGEMENT

This research was supported by National Science Foundation Grant No. GI-29932.

BIBLIOGRAPHY

1. Boersma, J., "Computation of Fresnel Integrals," Math. Comp.," 14, 380, 1960.

2. Canitez, N. and M. N. Toksöz, "Static and Dynamic Study of Earthquake Source Mechanism: San Fernando Earthquake," J. Geophys. Res., 77, 2583-2594, 1972.

3. Eshelby, J. D., "The Elastic Field of A Crack Extending Non-uniformly under General Anti-plane Loading," J. Mech. Phys. Solids, 17, 177-199, 1971.

4. Haskell, N. A., "Elastic Displacements in the Near-Field of a Propagating Fault," Bull. Seism. Soc. Am., 59, 865-908, 1969.

5. Haskell, N. A. and K. C. Thomson, "Elastodynamic Near-field of a Finite Propagating Tensile Fault, "Bull. Seism. Soc. Am.," 62, 675-698, 1972.

6. Mal, A. K., "Rayleigh Waves from a Moving Thrust Fault," Bull. Seism. Soc. Am., 62, 751-762, 1972.

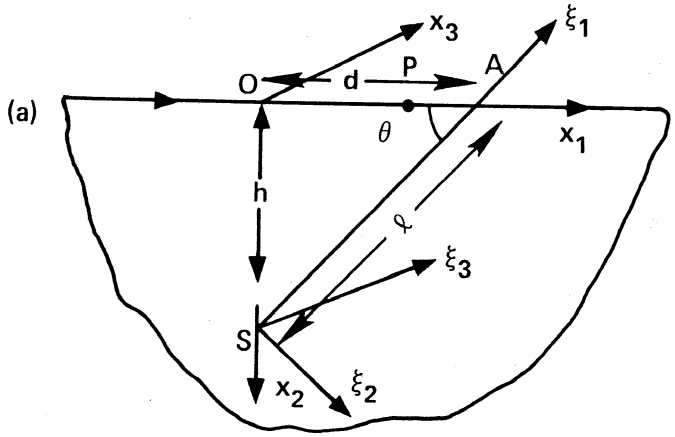

Figure 1(a). Geometry of the Problem

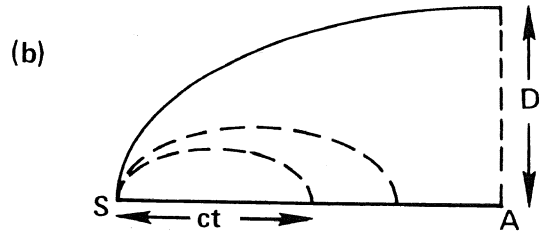

Figure 1(b). Shape of the Running Shear Failure